ORIGINAL PAPER

RJME
Romanian Journal of Morphology & Embryology
http://www.rjme.ro/

In vivo biodistribution of CNTs using a BALB/c mouse experimental model

MARIANA OANA MIHAELA FUFĂ[1,2)], DAN EDUARD MIHAIESCU[3)], LAURENŢIU MOGOANTĂ[4)], TUDOR-ADRIAN BĂLŞEANU[5)], GEORGE DAN MOGOŞANU[6)], ALEXANDRU MIHAI GRUMEZESCU[1)], ALEXANDRA BOLOCAN[7)]

[1)]*Department of Science and Engineering of Oxide Materials and Nanomaterials, Faculty of Applied Chemistry and Materials Science, Politehnica University of Bucharest, Romania*

[2)]*Lasers Department, National Institute for Laser, Plasma and Radiation Physics, Magurele, Bucharest, Romania*

[3)]*Department of Organic Chemistry, Faculty of Applied Chemistry and Materials Science, Politehnica University of Bucharest, Romania*

[4)]*Research Center for Microscopic Morphology and Immunology, University of Medicine and Pharmacy of Craiova, Romania*

[5)]*Research Center for Clinical and Experimental Medicine, University of Medicine and Pharmacy of Craiova, Romania*

[6)]*Department of Pharmacognosy & Phytotherapy, Faculty of Pharmacy, University of Medicine and Pharmacy of Craiova, Romania*

[7)]*Emergency University Hospital, Bucharest, Romania; "Carol Davila" University of Medicine and Pharmacy, Bucharest, Romania*

Abstract

Background: Due to their unique behaviors, carbon nanotubes (CNTs)-based systems meet essential requirements for modern applications, such as electronics, optics, photovoltaics, fuel cells, aerospace engineering, military and biomedical applications. CNTs biocompatibility and toxic effects were assessed both *in vitro* and *in vivo*, in terms of hemocompatibility, cytocompatibility, immunoreactions and genetic behavior. *Aim*: The aim of this paper is to evaluate the *in vivo* biodistribution and biocompatibility of carbon nanopowder synthesized by plasma processing, using a BALB/c mouse experimental model. *Materials and Methods*: Three months old BALB/c mice were aseptically injected with 100 µL of 1 mg/mL dispersions. The obtained carbon-based nano-systems were dispersed in saline solution and subsequently sterilized by using a 30 minutes treatment with UV irradiation. The reference mice were injected with 100 µL of saline. The mice were kept under standard conditions of light, temperature, humidity, food and water (*ad libitum*) before the vital organ harvest. The animal welfare was daily monitored. At two and 10 days after the inoculation, the animals were euthanized under general anesthesia, for the sampling of internal organs (brain, myocardium, pancreas, liver, lung, kidney and spleen). *Results*: No animal died during the experiment. Brain, myocardium and pancreas were histologically normal, with no tissue damage, inflammatory infiltrate or inorganic deposits. CNTs were evidenced only in hepatic, renal, pulmonary and spleen tissue samples. Increased amounts of inorganic granular structures were reported after 10 days of treatment, when compared to the short-term (two days) inoculation. *Conclusions*: Our BALB/c mouse experimental model was found to be useful for the *in vivo* assessment of biodistribution and biocompatibility of CNTs.

Keywords: carbon nanopowder, CNTs, plasma processing, in vivo, mice, biodistribution.

Introduction

Even if there is still short time since the carbon nanotubes (CNTs) have been discovered, substantial research studies have been performed with respect to their structural features, physical and chemical properties and potential applications. Given the specific tubular morphology obtained by rolling the graphene sheets that contain within their structure highly oriented hexagonal architectures of sp^2 hybridized carbon, one-dimensional CNTs possess specific unique strength and stability (when compared to sp^3 bonds found in other carbon allotropes) and singular tunable properties (thanks to the peculiar electronic structure) [1–4].

When referring to the carbon-based tube classification, there are two distinct criteria: chirality and constituent graphitic sheets. (*a*) If considering the wrapping vector [given by the carbon atoms orientation to each other and denoted by (*n*,*m*) pairs of integer values] and the θ chiral angle (which values are comprised between 0 and $\pi/6$), one can identify the armchair (tubes with $m=n$ and $\theta=30^0$ that have purely metallic behavior), zig-zag (tubes with $m=0$ and $\theta=0^0$ that have semiconductor behavior) and chiral (tubes with $m\neq n$ and $0^0<\theta<30^0$) carbon nanotubes [1, 3, 5, 6]. (*b*) When considering the constituent graphene layers, the single-walled, double-walled and multi-walled are identified [2, 7, 8].

Regarding the synthesis of CNTs, three major strategies succeeded and are intensively used during experimental procedures: (*a*) the chemical vapor deposition that involves simultaneous high temperature treatments of highly pure gaseous or liquid carbonaceous precursor and transition metal catalysts [9–11]; (*b*) the arc discharge, which requires a high electric potential between two carbon-based electrodes [12, 13]; and (*c*) the laser ablation approach that involves concurrent evaporation–condensation phenomena of graphite and metallic catalyst [4, 14, 15]. The above-mentioned synthesis approaches represent standard

directions towards the production of wide-ranging CNTs (in terms of structural, morphological and dimensional aspects) thanks to their mutual features, such as high synthesis yield, short-time processes, facile adjustment of process parameters and reproducible results. Other synthesis strategies experienced for carbon nanotube fabrication include ball milling [16, 17], hydrothermal method [18, 19], electrolysis [20, 21] and microwave-assisted synthesis [22, 23].

Given the particular structural, morphological and dimensional features of carbon nanotubes, these structures possess genuine physical properties (in terms of stiffness and hardness, tensile and flexural strength, wettability, optical properties, thermal and electric conductivity) and chemical properties (in terms of chemical reactivity and surface chemical versatility). Thus, CNTs-based systems have unique behaviors and meet essential requirements for modern world applications, such as electronics [24–29], optics [30–32], photovoltaics [33–35], fuel cells [36–38], aerospace and automotive engineering [39–41], military and ballistics [42–45], and biomedical applications [46–48]. It is also necessary to state that the above-mentioned applicative directions of carbon-based nanostructures represent a relevant part of CNTs-based research activity, but is not limited to them.

Since the biomedical-related direction of carbon nanotubes involves inevitable interactions with living structures, it is necessary to evaluate their pathophysiological behavior in human simulated environments, human-derived cell cultures and animal models. Thereby, various recent research studies have assessed CNTs biocompatible or toxic effects, in both *in vitro* and *in vivo* experiments. Given the increased acknowledged cytotoxic activity of pristine carbon nanotubes against various cells and tissues, the research community turned its attention towards the development of high purity functionalized CNTs, which can successfully be used for novel biomaterial and biodevice fabrication. Thus, plenty research studies have extensively examined the *in vitro* activity of functionalized carbon nanotubes, in terms of hemocompatibility [49–52], cytocompatibility [53–58], immune reactions [59–61] and genetic behavior [62–64]. When it comes to living organism interactions and *in vivo* behavior, the recently performed experimental studies have evaluated CNTs-based materials in terms of biodistribution and biocompatibility [56, 65–68], acute and chronic local or systemic reactions [69–72] and genotoxicity [73, 74].

The aim of this paper is to evaluate the *in vivo* biodistribution and biocompatibility of CNTs synthesized by plasma processing.

Materials and Methods

In vivo biodistribution of CNTs

Synthesis by plasma processing and characterization of CNTs were presented in a previous paper [75].

The experimental protocol was applied according with the European Council Directive No. 86/609 (November 24, 1986), the European Convention for the Protection of Vertebrate Animals used for Experimental and Other Scientific Purposes (December 2, 2005), and the Romanian Parliament Law No. 43 (April 11, 2014) on the protection of animals used for scientific purposes. The study was approved by the Ethics Committee of the University of Medicine and Pharmacy of Craiova, Romania (Approval Report No. 118/27.05.2015).

In order to assess the *in vivo* compatibility and distribution of the synthesized nanostructures, three months old BALB/c mice were aseptically injected with 100 μL of 1 mg/mL dispersions. The obtained carbon-based nanosystems were dispersed in saline solution and subsequently sterilized by using a 30 minutes treatment with UV irradiation. The intravenous administration of the as-prepared dispersions was carried out slowly into the left jugular vein, using a catheter (before the inoculation, the mice were subjected to general anesthesia by the intraperitoneal injection of a Ketamine/Xylazine mixture). The reference mice were injected with 100 μL of saline [76].

The mice were kept under standard conditions of light, temperature, humidity, food and water (*ad libitum*) before the vital organ harvest. The animal welfare was daily monitored. No animal died during the experiment. At two and 10 days after the inoculation, the animals were euthanized under general anesthesia, for the sampling of internal organs (brain, myocardium, pancreas, liver, lung, kidney and spleen). After the organ sampling, the biological material was washed in phosphate-buffered saline (PBS), then fixed in 10% buffered neutral formalin (for 72 hours, at room temperature) and processed for microscopic histology studies [76].

Serial sections with 4 μm thickness were obtained considering the prepared organs, by using a MICROM HM355s rotary microtome (MICROM International GmbH, Walldorf, Germany) equipped with a waterfall-based section transfer system (STS, MICROM). The cross-sections were placed on histological blades treated with poly-L-Lysine (Sigma-Aldrich, Munich, Germany). After Hematoxylin–Eosin (HE) classical staining, the obtained cross-sections were evaluated and photographed by using a Nikon Eclipse 55i light microscope equipped with a Nikon DS–Fi1 CCD high definition video camera (Nikon Instruments, Apidrag, Romania). The concerned images were captured, stored and analyzed by using the Image ProPlus 7 AMS software (Media Cybernetics Inc., Marlow, Buckinghamshire, UK) [77].

Results

In vivo biocompatibility and biodistribution of CNTs after two days treatment

Brain

The lower magnification of brain tissue sample harvested after two days of carbon-based nanostructures treatment shows specific aspects of cerebral cortex. As it can be observed starting from the right side of the obtained image, one can clearly distinguish the three specific layers of cerebral cortex: (*a*) the molecular layer (the most superficial layer of the neocortex that consists in a dense zone that mostly contains dendritic and axonal synapses, but also few nuclei belonging to the supportive and protective glial cells), (*b*) the outer granular layer (the second layer of the cerebral cortex that consists in a dense population of neuronal synapses, stellate cells and small pyramidal cells with specific bulky and triangle-like

nuclei) and (*c*) the outer pyramidal cell layer (the cerebral zone containing mostly moderate sized pyramidal cells and Martinotti cells). Also, one can distinguish the typical features assigned to the abundant prominent spherical glial cells. At a higher magnification of the tissue sample, it can be observed that few regular capillaries with specific morphological and dimensional sane erythrocytes were capture in cross-section (Figure 1a).

Myocardium

The obtained micrographs corresponding to the prepared cardiac muscle sample capture the specific branched arrangement of cardiac fibers. Given the characteristic rotation of constituent protein filaments, the observed muscular fibers possess specific striated aspect within their morphology. The identified myocardiocytes possess specific single and central round-oval nuclei. Several capillaries are captured in the obtained images and no histological modifications are reported regarding their morphology. It is important to notice the significant amount of red blood cells within the identified capillaries, but also their specific histological aspects (as a result of the physiological cardiac activity). At higher magnification, one can also clearly observe few intercalated discs, which are specialized junctions established between adjacent cardiac muscle cells (Figure 1b).

Pancreas

The first histological examination of pancreatic tissue sample reveals the specific distribution of exocrine pancreatic acinar cells in whose dense mass are specifically identified two hormone secretory Langerhans islets. The identified prominent acinar cells have unique heterochromatic nuclei with round-oval morphology and possess particular secretory eosinophilic granules at the apical pole. Several blood vessels are captured in cross-section and one can clearly notice that they are supplied with a large number of normal aspect red blood cells. At a higher magnification, detailed aspects related to the endocrine pancreatic tissue are revealed: pale epithelial cells with specific reduced affinity to the used staining protocol that have single central oval nuclei. Also, the identified pancreatic capillaries and insulo-acinar portal system show normal histological aspects and a significant amount of healthy red blood cells content, as a result of the physiological pancreatic function (Figure 1c).

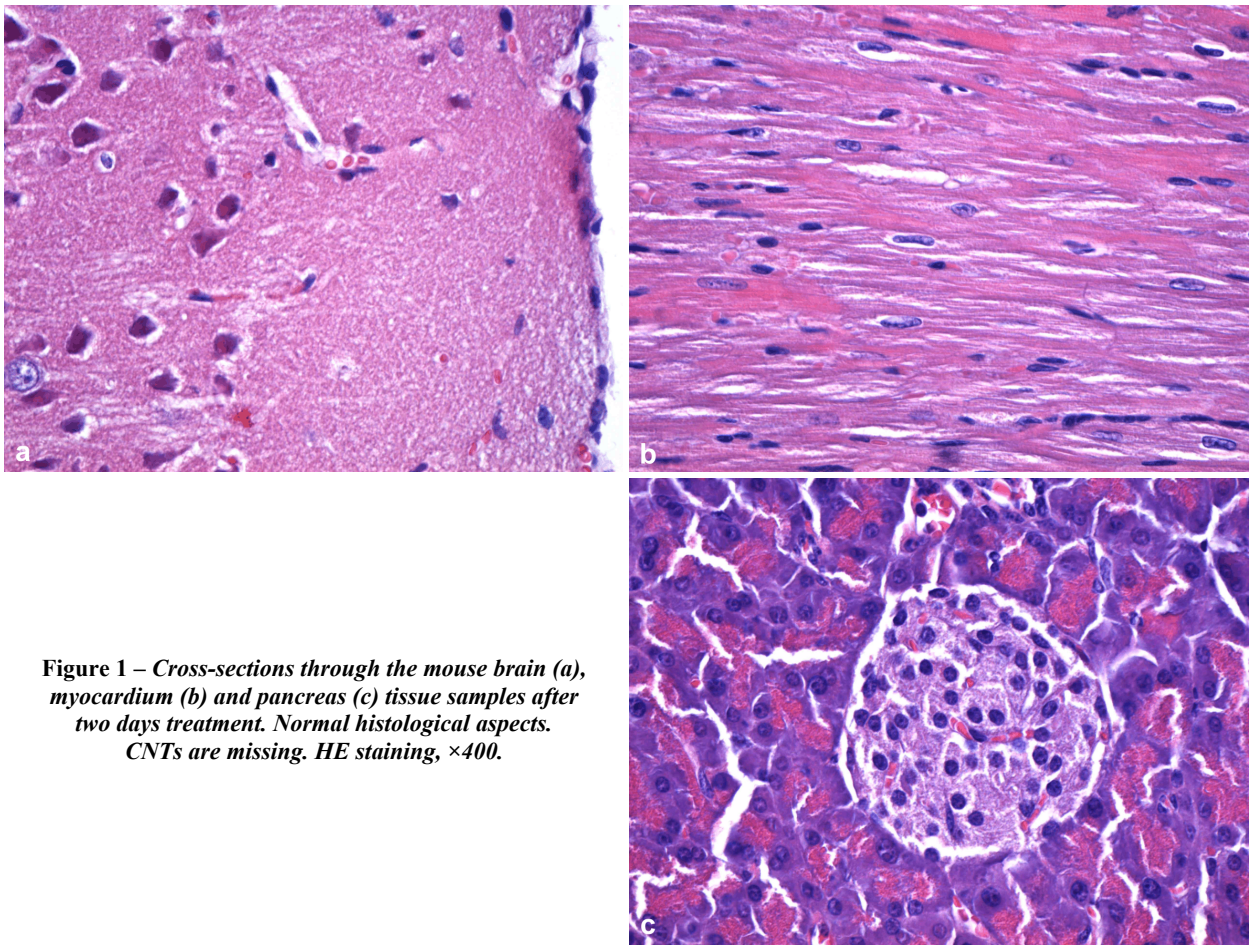

Figure 1 – ***Cross-sections through the mouse brain (a), myocardium (b) and pancreas (c) tissue samples after two days treatment. Normal histological aspects. CNTs are missing. HE staining, ×400.***

Liver

At reduced microscopic magnification of the hepatic tissue sample one can notice typical aspects: polyhedral shaped hepatocytes disposed within highly arranged cords that have specific prominent spherical euchromatic nuclei. Few isolated erythrocytes are observed inside the longitudinally captured hepatic capillaries and a significant amount of red blood cells are noticed within the centrilobular veins captures in cross-section. On the other hand, when considering the increased magnified histological images, except for the presence of major uninucleate and few binucleate hepatocytes, several atypical aspects are observed: inside the blood vessels and peripheral Kupffer cells of the hepatic capillaries important dark brown

agglomerated structures are identified. The identified aspects suggest that the mentioned specialized hepatic macrophages have a specific intense activity, but also recognize and engulf the carbon-based foreign nanostructures during their effort to protect the liver. As one can observe, the nanostructure density inside the cells depends on the capillary dimension of the hepatic parenchyma (Figure 2, a and b).

Kidney

Regarding the histological aspects of the renal tissue sample, one can clearly notice that no morphological alterations are reported with respect to the constituent tissue, except for the cross-section captured large blood vessels. According to the obtained images, specific histological aspects corresponding to the renal cortex can be observed: one can identify the proximal convoluted (the single layered regions with a narrow lumen defined by few cubic epithelial cells) and distal convoluted (the single layered regions with a wide lumen defined by several cubic epithelial cells) uriniferous tubules, but also the prominent renal glomerulus. At a closer look, one can distinguish that the urinary space is clearly defined between the parietal (simple squamous epithelium) and visceral (podocyte-based) layers of Bowman's capsule, but also that the intraglomerular mesangial cells have specific histological aspects (monocyte-derived or smooth muscle-derived mural cells with singular prominent round-oval nuclei). Also, several typically shaped and sized erythrocytes are captured within the capillaries of the renal glomerulus, which may indicate a normal physiological function. As mentioned above, several darkish voluminous aggregate structures are noticed inside the large renal blood vessels, which can suggest that the inoculated structures do not satisfy the required conditions for renal excretion (Figure 2, c and d).

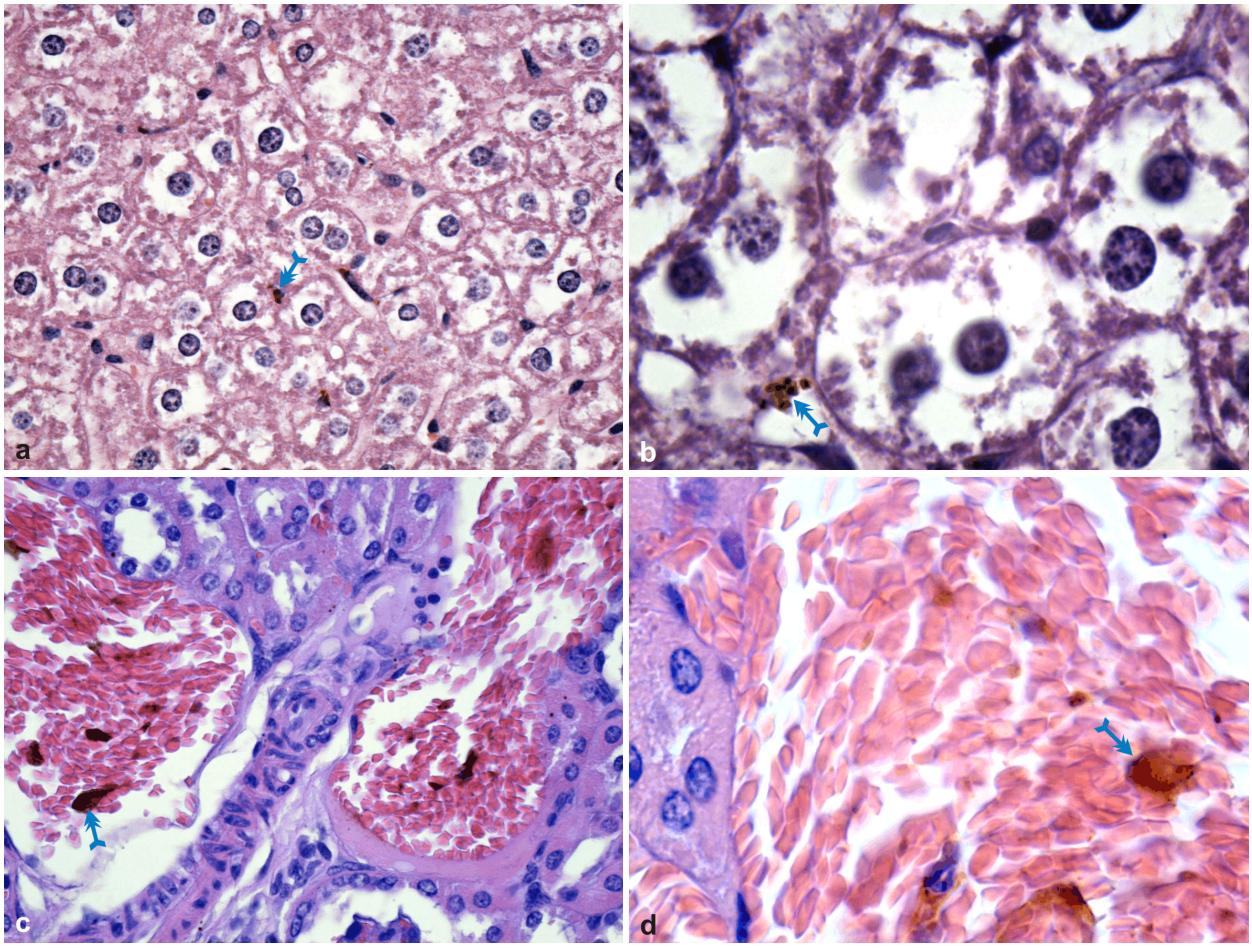

Figure 2 – ***Cross-sections through the mouse liver (a and b) and kidney (c and d) tissue samples after two days treatment. CNTs were highlighted as prominent dark brown granular aggregates. HE staining: (a and c) ×400; (b and d) ×1000.***

Lung

When considering the histological aspects of the pulmonary tissue sample analyzed after a two days treatment, one can distinguish specific aspects corresponding to pulmonary alveoli that mostly contain within their structure type 1 pneumocytes (flattened squamous cells, which define the alveolar sacs) and isolated type 2 alveolar cells (spherical prominent cells with foamy cytoplasm and unique round nuclei located within the alveolar septal junctional zones). Also, it can be observed the significant amount of specifically disk-shaped erythrocytes inside the captured alveolar capillaries. On the other hand, within the perivascular and alveolar septa macrophages one can observe the presence of prominent dark brown granular aggregates, because of monocyte endocytosis. Several isolated low-dimensional agglomerates can also be observed around the cells located inside the vascular lumen. Also, it can be observed that some of the pulmonary alveoli have atypical cellular content and alveolar septa, which can indicate the presence of inflammatory or fibrotic damage (Figure 2, e and f).

Spleen

With respect to the splenic tissue, histological alterations are observed even after a two days treatment. Due to an intense activity required during the formation of multi-lobed macrophages, one can notice significant hypertrophy of the splenic white pulp. Also, typical histological aspects of the splenic red pulp are clearly identified (the cellular cords composed by endothelial cells with prominent spherical-ellipsoidal shaped nuclei specifically delimit splenic sinusoids), but within this constituent region of the spleen one can observe significant dark brown deposits. The identified aggregate structures have sphere-like morphology and variable dimensions (less than 3 μm) and are located within the macrophage system cells, which belong both to Billroth cords and sinusoid capillaries (Figure 2, g and h).

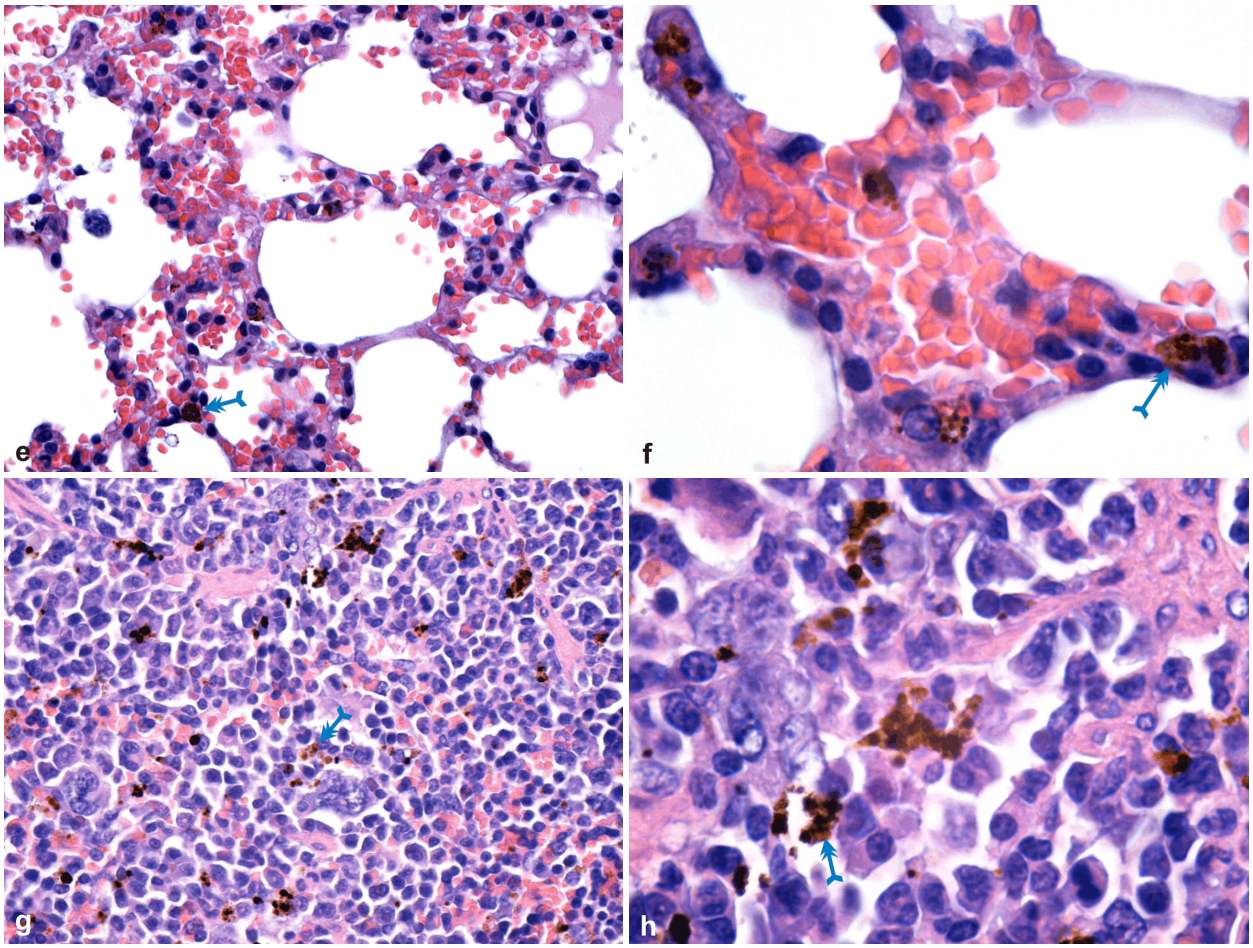

Figure 2 (continued) – ***Cross-sections through the mouse lung (e and f) and spleen (g and h) tissue samples after two days treatment. CNTs were highlighted as prominent dark brown granular aggregates. HE staining: (e and g) ×400; (f and h) ×1000.***

In vivo biocompatibility and biodistribution of CNTs after 10 days treatment

Brain

Starting from the superior region, of the lower magnification, histological image corresponding to the brain tissue fragment harvested after a 10 days treatment, one can observe the specific distribution of the plexiform, outer granular and outer pyramidal cell layers of the cerebral cortex. When analyzing most closely the concerned tissue sample, specific aspects of abundant neuroglia can be noticed: prominent cells with typical vesicular aspect, spherical morphology and euchromatic large nuclei (the finely dispersed pale chromatin is the result of an intense synthesis activity) that have considerable single nucleolus or double nucleoli within an eosinophilic cytoplasm. Also, the microscopic slide captures few blood vessels (either in longitudinal or cross-section) with significant red blood cell content. The morphological, dimensional and visual aspects of the concerned blood cells correspond to healthy, unaffected and physiological features of erythrocytes (Figure 3a).

Myocardium

When considering the myocardial tissue sample harvested after 10 days of *in vivo* experimental treatment, the prepared histological slide also shows normal aspects. Thus, one can observe the specific branch-like distribution of striated cardiac fibers, but also the unique central heterochromatic nuclei belonging to constituent cardiomyocytes. Also, it can be noticed that the constituent nuclei possess a specific stubby aspect and lie in a rather granular cytoplasm. Several blood vessels with significant hematic supply are also observed within the concerned histological slides. The captured erythrocytes possess typical oval biconcave disk shape, with no indications regarding their potential alteration or damage (Figure 3b).

Pancreas

The obtained images of the harvested pancreatic tissue sample show specific aspects correlated to healthy and proper functioning exocrine and endocrine pancreatic structures. The exocrine pancreatic tissue consists in specific pancreatic acini (epithelial cubic cells distributed in a single layer around the intercalated ducts) with normal appearance centro-acinar cells (polarized cells with intense eosinophilic aspect at the secretory apical pole and basophilic aspect at the basal pole, that possess unique round-oval nuclei with central single or multiple nucleoli). The enhanced affinity of the acinar pancreatic cells for the eosin staining is due to the abundant protein content of the exocrine secretory granules, which provides as significant data about the normal exocrine secretory function of the pancreas. Also, a specific Langerhans islet is captured within the obtained images, such that one can distinguish the endocrine epithelial cells with oval unique central nuclei, but also we can notice aspects that indicate a normal physiological blood supply (Figure 3c).

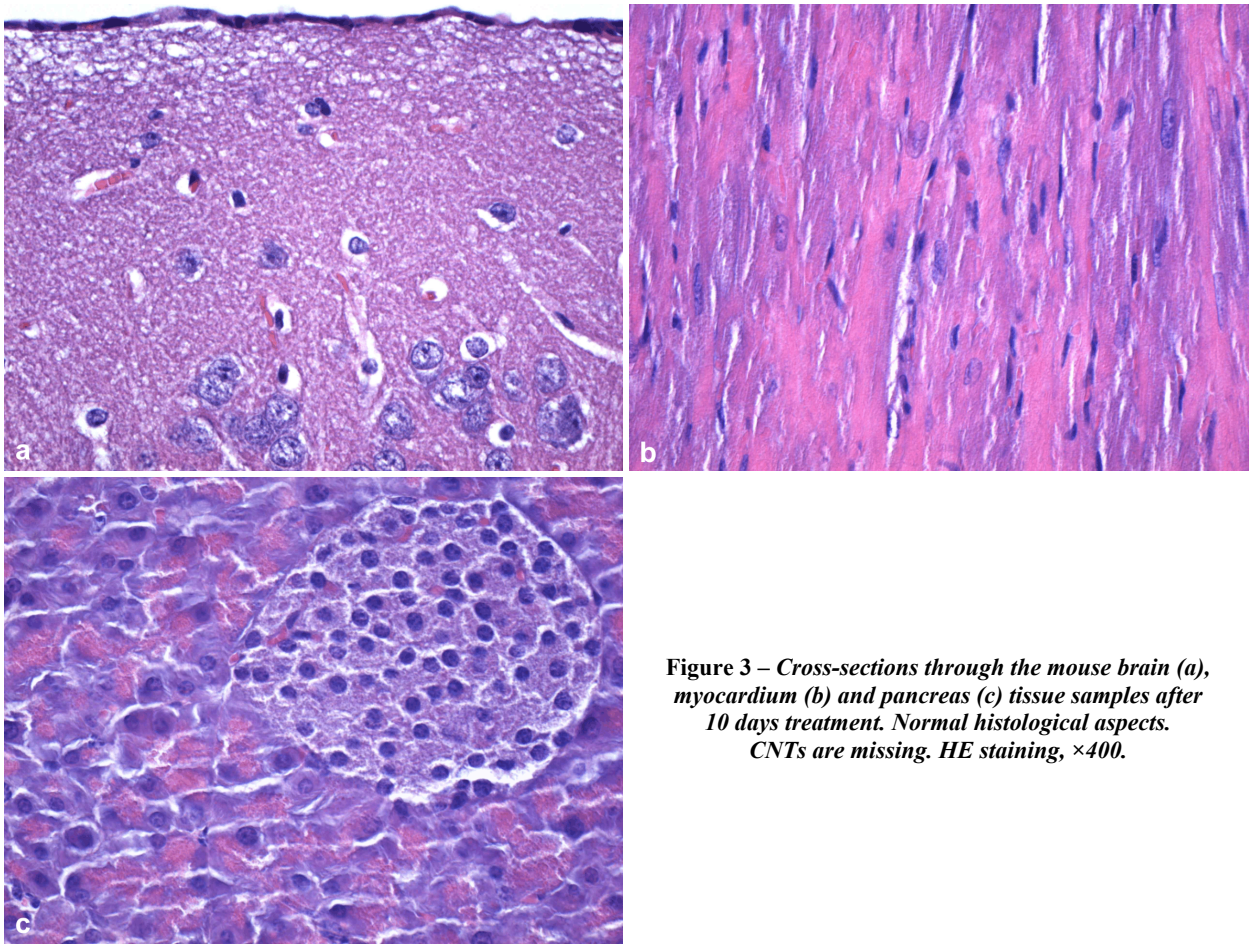

Figure 3 – ***Cross-sections through the mouse brain (a), myocardium (b) and pancreas (c) tissue samples after 10 days treatment. Normal histological aspects. CNTs are missing. HE staining, ×400.***

Liver

After the long-time treatment of the mice, the harvested hepatic sample showed specific foreign granular aggregates even at lower magnification. A large centrilobular hepatic vein and several hepatic capillaries are captured in cross-section, respectively in longitudinal section. All the identified erythrocytes within the blood vessels have specific aspects (in terms of color, dimension and shape), but significant dark brown structures are noticed between them. Also, at higher magnifications, one can observe that the hepatocytes still possess typical aspects (polygonal parenchymal hepatic cells with prominent euchromatic nuclei), but important sphere-like aggregates are reported within the centrilobular Browicz–Kupffer macrophage cells. One can presume that the intravenous inoculation of the carbon-based nanostructures induce the carrier-like role of the bloodstream. When reaching the hepatic stage, the mononuclear phagocyte system of the liver consequently acts against the identified foreign structures, encouraging thus the specific recognition and engulfing of the inoculated nanosystems (Figure 4, a and b).

Kidney

At lower magnification of the kidney tissue sample harvested after 10 days treatment, one can observe the disposal of single-layered cuboidal epithelium with central prominent nuclei into cellular cords that specifically delimit normal histological proximal and distal convoluted renal tubules. Also, two renal glomeruli are noticed and the few atypical dark colored structures are identified within the large dimension blood vessel captured in cross-section. When considering the higher magnification image, it can be observed that the renal glomerulus is clearly defined by the Bowman's capsule and that the glomerular vascular bundle is discernable and properly vascularized (the significant amount of unaltered red blood cells within the glomerular capillaries may suggest an intense excretory

activity of the treated kidney). Regarding the cross-section captured blood vessel, several dark brown voluminous and few reduce-sized agglomerates can be noticed within. One can also notice that the lower foreign structures seem to be located onto or into the red blood cells. Thus, one can assume either that the inoculated nanostructured does not match the specific requirements for renal elimination or that only pristine and non-aggregated carbonaceous materials may be susceptible to renal excretion (Figure 4, c and d).

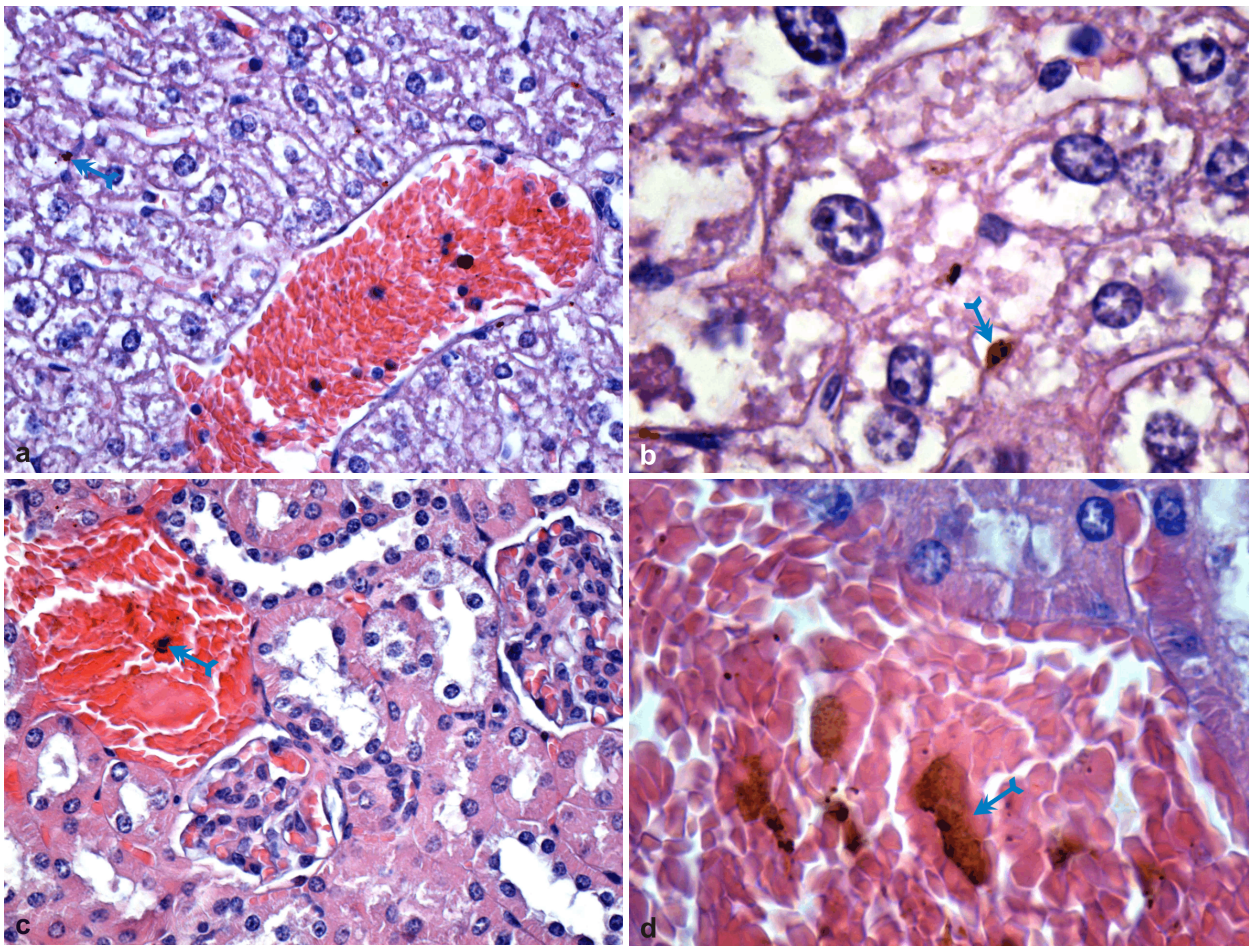

Figure 4 – ***Cross-sections through the mouse liver (a and b) and kidney (c and d) tissue samples after 10 days treatment. CNTs were highlighted as prominent dark brown granular aggregates. HE staining: (a and c) ×400; (b and d) ×1000.***

Lung

With respect to the histological aspects of the pulmonary tissue sample, one can mention that the lower magnification obtained image shows several pulmonary alveoli with specific type 1 flattened alveolar epithelial cells and type 2 spherical alveolocytes. Mostly, within the perivascular macrophages, one can observe massive amounts of darkish granular structures, while the reduced aggregates are located within the alveolar septal junctions. Given the central captured pulmonary alveolar structure, one can notice an atypical thickened alveolar septum and unspecific pulmonary and red blood cells inside the alveolus. One can thus presume that the pulmonary immune system had an intense and prolonged activity, which led to the partial fibrosis of pulmonary alveolar septum. This assumption can also be supported when considering the adjacent alveolar structures, which also seem to be affected by fibrotic and infiltrative inflammatory processes. Regarding the higher magnification histological image, it can be clearly observed that the large amount of biconcave disk-shaped erythrocytes from the right superior region is located within the pulmonary alveolus. Also, the preferential presence of the inoculated nanostructured within the perivascular region of the pulmonary tissue and the infiltrative inflammatory activity are indisputable underlined by this histological image (Figure 4, e and f).

Spleen

When considering the splenic treated sample, the obtained lower magnified image reveals important histological modifications with respect to the white pulp of spleen parenchyma: the central germination center is surrounded by a severe hypertrophic area, due to the excessive stimulation of lymphocyte activity required during macrophage activation. A significant amount of granular agglomerated structures is distributed within the splenic white pulp, inside the Billroth cords and splenic capillaries. Also, within the longitudinal captured sinuses, few isolated erythrocytes with darkish low-dimensioned aggregates onto or inside them can be observed. The higher magnification of the concerned splenic sample shows the specific granular aspect of the formed deposits, which have specific brown yellow or dark brown color, sphere-like morphology and micron dimensions (Figure 4, g and h).

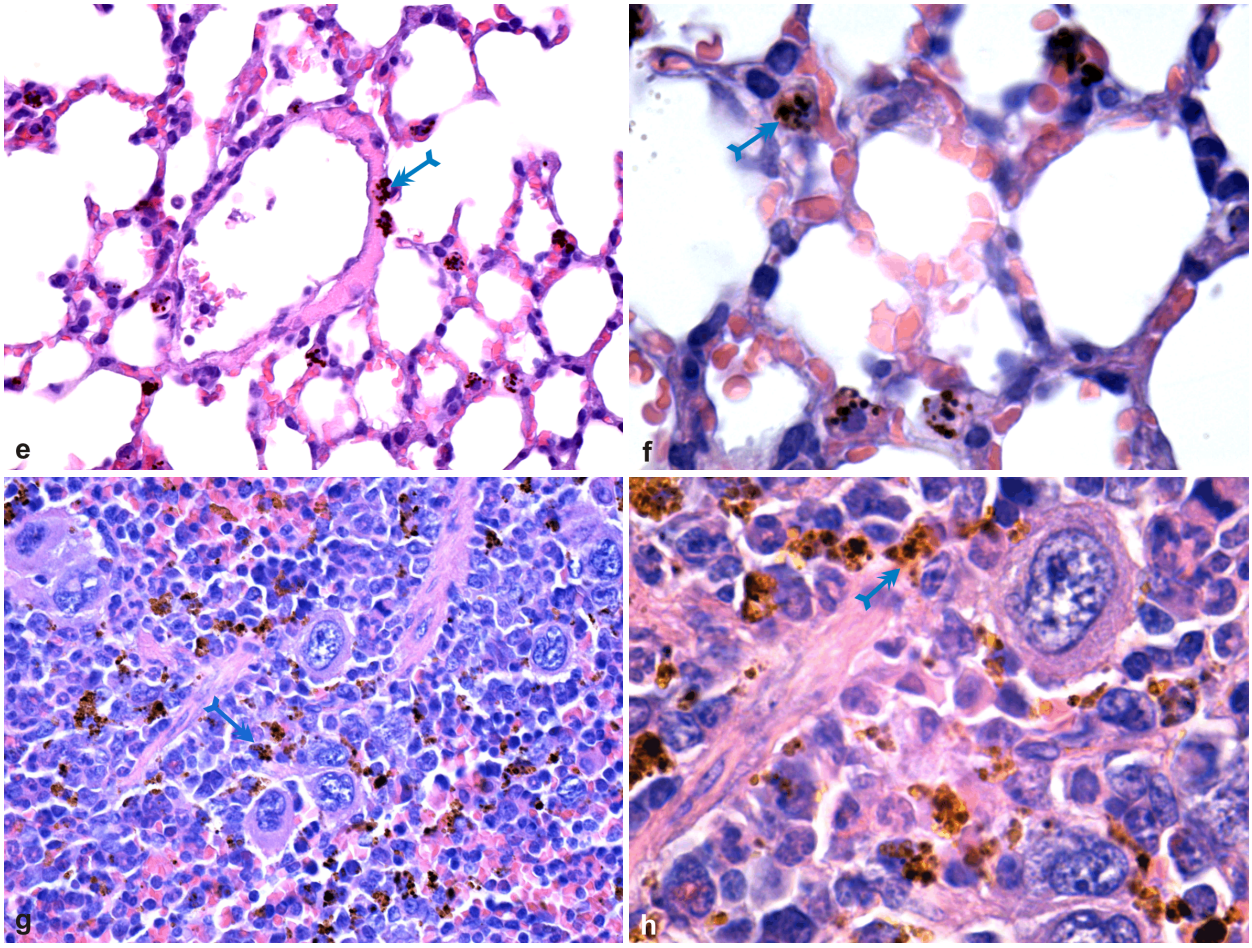

Figure 4 (continued) – ***Cross-sections through the mouse lung (e and f) and spleen (g and h) tissue samples after 10 days treatment. CNTs were highlighted as prominent dark brown granular aggregates. HE staining: (e and g) ×400; (f and h) ×1000.***

Discussion

Irrespective of the selected synthesis method, the produced CNTs may present many impurities (such as amorphous carbon, carbon nanoparticles, graphite sheets, fullerene structures or metallic catalyst particles) or defects (five or seven atom aromatic structures or graphene layer interruption) within their structure. Thereby, in order to produce CNT-based systems and novel materials for potential applications, it is mandatory to perform advanced purification of the synthesized nanostructures [78–80].

The CNTs physical purification methods usually require separation strategies and they do not affect the specific conjugated electronic structure. Among the physical approaches successfully used for carbon nanotubes purification, one must mention chromatographic technique [78, 80, 81], centrifugation [82–84], microfiltration [85, 86], microwave radiation [87, 88] or sonication [79].

When considering the chemical purification approach, several specific functionalization strategies are identified such as non-covalent, covalent and intrinsic defects functionalization. (*a*) The non-covalent modification of carbon nanotubes involves specific physically guided adsorption phenomena of macromolecules onto the surface of the tube, thanks to van der Waals and π–π interactions. By considering this particular functionalization strategy, several organic compounds have been successfully adsorbed to the CNTs surface, such as various ionic, non-ionic or Gemini surfactants [89–91], polymers [92–94] and distinct biomacromolecules [95, 96]. (*b*) The covalent functionalization of carbon nanotubes specifically involves chemical reactions towards the double bonds within the carbon layer, which significantly affects the electronic structure of the CNTs [97–102]. (*c*) The specific functionalization of structural defects within the outer wall of the CNTs usually implies oxidation or redox reactions in the presence of gaseous or liquid oxidizing circumstances. The particular use of chemical agents in carbon-based nanotube purification implies simultaneous phenomena of impurity removal and functional group formation (such as hydroxyl, carboxyl, carbonyl, amine, thiol, ester, epoxy), which require either passive chemical reactions in gaseous or aqueous media or electrochemical processes. When referring to this particular strategy, successful results for liquid state purification have been reported for the following chemical compounds (but not limited to): aspartic acid [103], ammonium hydroxide and hydrogen peroxide [104], citric acid [105, 106], hydrochloric acid [107], *meta*-chloroperoxybenzoic acid [108], N-hydroxysulfosuccinimide and 1-ethyl-3-[3-dimethylaminopropyl]carbodiimide hydrochloride [109], nitric acid [110, 111], sulfuric acid [112], pyrene derivates [113], sodium hydroxide [114], sodium and potassium chloride [115], tetraethylenepentamine [116], 3-aminopropyltriethoxysilane [117, 118],

4-aminobenzoic acid [119] or various reactive mixtures [60, 120–123].

For biomedical applications, it is mandatory to engineer biocompatible and high purity CNTs with increased stability and enhanced dispersion in commonly used inorganic and organic bio-related solvents. The tremendous progress lately reported in novel technologies, the genuine physicochemical versatility and surface chemical reactivity of carbon-based nanotubes offer impressive possibilities to develop novel CNTs-based composite and hybrid materials for promising biomedical application. Therefore, recent studies performed with respect to the particular domain of modern healthcare practice have reported promising results regarding the use of CNTs-based materials as attractive tools for biosensing [46, 124–129], bioimaging [130–133], drug delivery [134–136], tissue engineering [137–141], cancer therapy [48, 142–145], degenerative conditions therapy [146–148] and genetic therapy [149–151].

After two and 10 days treatment with carbon-based nanostructures, using a BALB/c mouse experimental model, the histological aspects reported for the myocardial and pancreatic tissues were physiologically normal, with no presence of tissue damage, inflammatory infiltrate or inorganic deposits. Among the investigated vital organs, the myocardium and the pancreas does not possess a specific native defense system, so as one can assume that the presence of the synthesized systems within the supplied bloodstream is not enough to produce cellular internalization and subsequent cell injury. Although the other concerned organs specifically possess an intrinsic immune response system, no modifications were observed with respect to the cerebral tissue. Given the normal histological aspects, which were noticed when considering the microscopic slides analysis, one can thus presume that the inoculated carbonaceous nanosystems do not pass through the blood–brain barrier. Significant darkish granular structures were instead present within the blood vessels of the renal tissue samples. Except for the identified deposits, the histological aspects corresponding to the renal cortex were physiological normal, indicating thus either that the carbon tubes are not suitable for renal elimination or that only extremely reduced and non-aggregated nanosystems are suitable for renal excretion. Regarding the hepatic tissue samples, significant agglomerate structures were identified within the Kupffer macrophage cells for both treatments, suggesting that the mononuclear phagocyte system of the liver intensely reacted when the carbon-based nanostructures carried by the bloodstream attained this tissue. The pulmonary tissue seemed to be significantly affected by the applied treatment, since except for the massive amounts of dark brown aggregate deposits that were observed in both perivascular and alveolar septal junction, one can also observed substantial modifications corresponding to inflammatory and fibrotic processed. Given the significant role of spleen within the lymphatic system, this organ represents the first defense structure against potential foreign structures. The histological aspects – splenic white pulp hypertrophy, important granular deposits within the Billroth cords and splenic sinusoids of the red pulp – reported after both treatments confirmed the above hypothesis. It is also important to mention that increased concentrations of inorganic granular structures were reported after the performed 10 days treatment, when compared to the short-term inoculation – within all the affected tissues corresponding to liver, lung, kidney and spleen.

Conclusions

The *in vivo* biodistribution and biocompatibility of CNTs were assessed using a BALB/c mouse experimental model. No animal died during the experiment. From the histological point of view, brain, myocardium and pancreas were physiologically normal, with no tissue damage, inflammatory infiltrate or inorganic deposits. CNTs were evidenced only in hepatic, renal, pulmonary and spleen tissue samples. Increased amounts of CNTs were reported after 10 days treatment, when compared to the short-term (two days) inoculation.

Conflict of interests

The authors declare that they have no conflict of interests.

References

[1] Dresselhaus MS. Carbon nanotubes. Carbon, 1995, 33(7): 871–872.
[2] Inagaki M, Radovic LR. Nanocarbons. Carbon, 2002, 40(12): 2279–2282.
[3] Ávila AF, Lacerda GSR. Molecular mechanics applied to single-walled carbon nanotubes. Mater Res, 2008, 11(3):325–333.
[4] Purohit R, Purohit K, Rana S, Rana RS, Patel V. Carbon nanotubes and their growth methods. Procedia Mater Sci, 2014, 6:716–728.
[5] Anantram MP, Léonard F. Physics of carbon nanotube electronic devices. Rep Progr Phys, 2006, 69(3):507–561.
[6] Yang F, Wang X, Zhang D, Yang J, Luo D, Xu Z, Wei J, Wang JQ, Xu Z, Peng F, Li X, Li R, Li Y, Li M, Bai X, Ding F, Li Y. Chirality-specific growth of single-walled carbon nanotubes on solid alloy catalysts. Nature, 2014, 510(7506):522–524.
[7] Őstling D, Tománek D, Rosén A. Electronic structure of single-wall, multiwall, and filled carbon nanotubes. Phys Rev B, 1997, 55(20):13980–13988.
[8] Su WC, Cheng YS. Carbon nanotubes size classification, characterization and nasal airway deposition. Inhal Toxicol, 2014, 26(14):843–852.
[9] De Greef N, Zhang L, Magrez A, Forró L, Locquet JP, Verpoest I, Seo JW. Direct growth of carbon nanotubes on carbon fibers: effect of the CVD parameters on the degradation of mechanical properties of carbon fibers. Diam Relat Mater, 2015, 51:39–48.
[10] Madani SS, Zare K, Ghoranneviss M, Monajjemi M, Salar Elahi A. Synthesis of carbon nanotubes using the cobalt nanocatalyst by thermal chemical vapor deposition technique. J Alloy Compd, 2015, 648:1104–1108.
[11] Rao R, Islam AE, Pierce N, Nikolaev P, Maruyama B. Chiral angle-dependent defect evolution in CVD-grown single-walled carbon nanotubes. Carbon, 2015, 95:287–291.
[12] Berkmans JA, Jagannatham M, Reddy RD, Haridoss P. Synthesis of thin bundled single walled carbon nanotubes and nanohorn hybrids by arc discharge technique in open air atmosphere. Diam Relat Mater, 2015, 55:12–15.
[13] Maria KH, Mieno T. Synthesis of single-walled carbon nanotubes by low-frequency bipolar pulsed arc discharge method. Vacuum, 2015, 113:11–18.
[14] Al-Hamaoy A, Chikarakara E, Jawad H, Gupta K, Kumar D, Rao MSR, Krishnamurthy S, Morshed M, Fox E, Brougham D, He X, Vázquez M, Brabazon D. Liquid phase-pulsed laser ablation: a route to fabricate different carbon nanostructures. Appl Surf Sci, 2014, 302:141–144.
[15] Radhakrishnan G, Adams PM, Bernstein LS. Plasma characterization and room temperature growth of carbon nanotubes and nano-onions by excimer laser ablation. Appl Surf Sci, 2007, 253(19):7651–7655.

[16] Nosbi N, Akil HM. Controlling the number of walls in multi walled carbon nanotubes/alumina hybrid compound *via* ball milling of precipitate catalyst. Appl Surf Sci, 2015, 340:78–88.
[17] Soares OSGP, Rocha RP, Gonçalves AG, Figueiredo JL, Órfão JJM, Pereira MFR. Easy method to prepare N-doped carbon nanotubes by ball milling. Carbon, 2015, 91:114–121.
[18] Manafi S, Rahaei MB, Elli Y, Joughehdoust S. High-yield synthesis of multi-walled carbon nanotube by hydrothermal method. Can J Chem Eng, 2010, 88(2):283–286.
[19] Zhang L, Hashimoto Y, Taishi T, Ni QQ. Mild hydrothermal treatment to prepare highly dispersed multi-walled carbon nanotubes. Appl Surf Sci, 2011, 257(6):1845–1849.
[20] Gupta RD, Schwandt C, Fray DJ. Preparation of tin-filled carbon nanotubes and nanoparticles by molten salt electrolysis. Carbon, 2014, 70:142–148.
[21] Schwandt C, Dimitrov AT, Fray DJ. High-yield synthesis of multi-walled carbon nanotubes from graphite by molten salt electrolysis. Carbon, 2012, 50(3):1311–1315.
[22] Mubarak NM, Sahu JN, Abdullah EC, Jayakumar NS, Ganesan P. Single stage production of carbon nanotubes using microwave technology. Diam Relat Mater, 2014, 48: 52–59.
[23] Wang Z, Wu Z, Di Benedetto G, Zunino JL III, Mitra S. Microwave synthesis of highly oxidized and defective carbon nanotubes for enhancing the performance of supercapacitors. Carbon, 2015, 91:103–113.
[24] Aïssa B, Nedil M, Habib MA, Abdul-Hafidh EH, Rosei F. High-performance thin-film-transistors based on semiconducting-enriched single-walled carbon nanotubes processed by electrical-breakdown strategy. Appl Surf Sci, 2015, 328:349–355.
[25] Bikshalu K, Reddy VSK, Reddy PCS, Rao KV. High-performance carbon nanotube field effect transistors with high *k* dielectric gate material. Mater Today Proc, 2015, 2(9 Pt A): 4457–4462.
[26] Jiang Y, Ling X, Jiao Z, Li L, Ma Q, Wu M, Chu Y, Zhao B. Flexible of multiwalled carbon nanotubes/manganese dioxide nanoflake textiles for high-performance electrochemical capacitors. Electrochim Acta, 2015, 153:246–253.
[27] Jung MJ, Jeong E, Lee YS. The surface chemical properties of multi-walled carbon nanotubes modified by thermal fluorination for electric double-layer capacitor. Appl Surf Sci, 2015, 347:250–257.
[28] Nam I, Bae S, Park S, Yoo YG, Lee JM, Han JW, Yi J. Omnidirectionally stretchable, high performance supercapacitors based on a graphene–carbon-nanotube layered structure. Nano Energy, 2015, 15:33–42.
[29] Trigueiro JPC, Lavall RL, Silva GG. Nanocomposites of graphene nanosheets/multiwalled carbon nanotubes as electrodes for In-plane supercapacitors. Electrochim Acta, 2016, 187:312–322.
[30] Li Z, Bai B, Li C, Dai Q. Efficient photo-thermionic emission from carbon nanotube arrays. Carbon, 2016, 96:641–646.
[31] Torres-Torres C, Mercado-Zúñiga C, Martínez-González CL, Martínez-Gutierréz H, Rebollo NR, Trejo-Valdez M, Vargas-García JR, Torres-Martínez R. Optical Kerr effect exhibited by carbon nanotubes and carbon/metal nanohybrid materials. Physica E, 2015, 73:156–162.
[32] Wu X, Yun M, Wang M, Liu C, Li K, Qin X, Kong W, Dong L. Numerical simulation of polarization beam splitter with triangular lattice of multi-walled carbon nanotube arrays. Opt Commun, 2015, 356:182–185.
[33] Abendroth T, Althues H, Mäder G, Härtel P, Kaskel S, Beyer E. Selective absorption of carbon nanotube thin films for solar energy applications. Sol Energy Mater Sol Cell, 2015, 143: 553–556.
[34] Lin JY, Wang WY, Chou SW. Flexible carbon nanotube/polypropylene composite plate decorated with poly(3,4-ethylenedioxythiophene) as efficient counter electrodes for dye-sensitized solar cells. J Power Sources, 2015, 282:348–357.
[35] Yu LP, Tune DD, Shearer CJ, Shapter JG. Implementation of antireflection layers for improved efficiency of carbon nanotube–silicon heterojunction solar cells. Sol Energy, 2015, 118:592–599.
[36] Huang J, Zhu N, Yang T, Zhang T, Wu P, Dang Z. Nickel oxide and carbon nanotube composite (NiO/CNT) as a novel cathode non-precious metal catalyst in microbial fuel cells. Biosens Bioelectron, 2015, 72:332–339.
[37] Kitahara T, Nakajima H, Okamura K. Gas diffusion layers coated with a microporous layer containing hydrophilic carbon nanotubes for performance enhancement of polymer electrolyte fuel cells under both low and high humidity conditions. J Power Sources, 2015, 283:115–124.
[38] Xie Z, Chen G, Yu X, Hou M, Shao Z, Hong S, Mu C. Carbon nanotubes grown *in situ* on carbon paper as a microporous layer for proton exchange membrane fuel cells. Int J Hydrogen Energy, 2015, 40(29):8958–8965.
[39] Asl MS, Farahbakhsh I, Nayebi B. Characteristics of multi-walled carbon nanotube toughened ZrB_2–SiC ceramic composite prepared by hot pressing. Ceram Int, 2016, 42(1 Pt B): 1950–1958.
[40] Jakubinek MB, Ashrafi B, Zhang Y, Martinez-Rubi Y, Kingston CT, Johnson A, Simard B. Single-walled carbon nanotube–epoxy composites for structural and conductive aerospace adhesives. Compos Part B Eng, 2015, 69:87–93.
[41] Wu G, Ma L, Liu L, Wang Y, Xie F, Zhong Z, Zhao M, Jiang B, Huang Y. Interfacially reinforced methylphenylsilicone resin composites by chemically grafting multiwall carbon nanotubes onto carbon fibers. Compos Part B Eng, 2015, 82:50–58.
[42] Farukh M, Singh AP, Dhawan SK. Enhanced electromagnetic shielding behavior of multi-walled carbon nanotube entrenched poly (3,4-ethylenedioxythiophene) nanocomposites. Compos Sci Technol, 2015, 114:94–102.
[43] Pandya KS, Naik NK. Analytical and experimental studies on ballistic impact behavior of carbon nanotube dispersed resin. Int J Impact Eng, 2015, 76:49–59.
[44] Wan Hanif WY, Risby MS, Noor MM. Influence of carbon nanotube inclusion on the fracture toughness and ballistic resistance of twaron/epoxy composite panels. Procedia Eng, 2015, 114:118–123.
[45] Zhang W, Xiong H, Wang S, Li M, Gu Y. Electromagnetic characteristics of carbon nanotube film materials. Chin J Aeronaut, 2015, 28(4):1245–1254.
[46] Baldo S, Buccheri S, Ballo A, Camarda M, La Magna A, Castagna ME, Romano A, Iannazzo D, Di Raimondo F, Neri G, Scalese S. Carbon nanotube-based sensing devices for human arginase-1 detection. Sensing Bio Sensing Res, 2015, Nov 26.
[47] Behnam B, Shier WT, Nia AH, Abnous K, Ramezani M. Non-covalent functionalization of single-walled carbon nanotubes with modified polyethyleneimines for efficient gene delivery. Int J Pharm, 2013, 454(1):204–215.
[48] Wen L, Ding W, Yang S, Xing D. Microwave pumped high-efficient thermoacoustic tumor therapy with single wall carbon nanotubes. Biomaterials, 2016, 75:163–173.
[49] Fent J, Bihari P, Vippola M, Sarlin E, Lakatos S. *In vitro* platelet activation, aggregation and platelet–granulocyte complex formation induced by surface modified single-walled carbon nanotubes. Toxicol *In Vitro*, 2015, 29(5):1132–1139.
[50] Gaffney AM, Santos-Martinez MJ, Satti A, Major TC, Wynne KJ, Gun'ko YK, Annich GM, Elia G, Radomski MW. Blood biocompatibility of surface-bound multi-walled carbon nanotubes. Nanomedicine, 2015, 11(1):39–46.
[51] Nie C, Ma L, Xia Y, He C, Deng J, Wang L, Cheng C, Sun S, Zhao C. Novel heparin-mimicking polymer brush grafted carbon nanotube/PES composite membranes for safe and efficient blood purification. J Membr Sci, 2015, 475:455–468.
[52] Zhao ML, Li DJ, Yuan L, Yue YC, Liu H, Sun X. Differences in cytocompatibility and hemocompatibility between carbon nanotubes and nitrogen-doped carbon nanotubes. Carbon, 2011, 49(9):3125–3133.
[53] Caballero-Díaz E, Guzmán-Ruiz R, Malagón MM, Simonet BM, Valcárcel M. Effects of the interaction of single-walled carbon nanotubes with 4-nonylphenol on their *in vitro* toxicity. J Hazard Mater, 2014, 275:107–115.
[54] Chen S, Hu S, Smith EF, Ruenraroengsak P, Thorley AJ, Menzel R, Goode AE, Ryan MP, Tetley TD, Porter AE, Shaffer MSP. Aqueous cationic, anionic and non-ionic multi-walled carbon nanotubes, functionalised with minimal framework damage, for biomedical application. Biomaterials, 2014, 35(17):4729–4738.
[55] Dinan NM, Atyabi F, Rouini MR, Amini M, Golabchifar AA, Dinarvand R. Doxorubicin loaded folate-targeted carbon nanotubes: preparation, cellular internalization, *in vitro* cytotoxicity and disposition kinetic study in the isolated perfused rat liver. Mater Sci Eng C Mater Biol Appl, 2014, 39:47–55.

[56] Dong C, Campell AS, Eldawud R, Perhinschi G, Rojanasakul Y, Dinu CZ. Effects of acid treatment on structure, properties and biocompatibility of carbon nanotubes. Appl Surf Sci, 2013, 264:261–268.

[57] Lobo AO, Corat MAF, Antunes EF, Ramos SC, Pacheco-Soares C, Corat EJ. Cytocompatibility studies of vertically-aligned multi-walled carbon nanotubes: raw material and functionalized by oxygen plasma. Mater Sci Eng C, 2012, 32(4):648–652.

[58] Zhang X, Zeng G, Tian J, Wan Q, Huang Q, Wang K, Zhang Q, Liu M, Deng F, Wei Y. PEGylation of carbon nanotubes *via* mussel inspired chemistry: preparation, characterization and biocompatibility evaluation. Appl Surf Sci, 2015, 351:425–432.

[59] Breznan D, Das D, MacKinnon-Roy C, Simard B, Kamurathasan P, Vincent R. Non-specific interaction of carbon nanotubes with the resazurin assay reagent: impact on *in vitro* assessment of nanoparticle cytotoxicity. Toxicol *In Vitro*, 2015, 29:142–147.

[60] Figarol A, Pourchez J, Boudard D, Forest V, Akono C, Tulliani JM, Lecompte JP, Cottier M, Bernache-Assollant D, Grosseau P. *In vitro* toxicity of carbon nanotubes, nanographite and carbon black, similar impacts of acid functionalization. Toxicol *In Vitro*, 2015, 30(1 Pt B):476–485.

[61] Pondman KM, Pednekar L, Paudyal B, Tsolaki AG, Kouser L, Khan HA, Shamji MH, Ten Haken B, Stenbeck G, Sim RB, Kishore U. Innate immune humoral factors, C1q and factor H, with differential pattern recognition properties, alter macrophage response to carbon nanotubes. Nanomedicine, 2015, 11(8):2109–2118.

[62] Antonioli E, Lobo AO, Ferretti M, Cohen M, Marciano FR, Corat EJ, Trava-Airoldi VJ. An evaluation of chondrocyte morphology and gene expression on superhydrophilic vertically-aligned multi-walled carbon nanotube films. Mater Sci Eng C Mater Biol Appl, 2013, 33(2):641–647.

[63] Lindberg HK, Falck GCM, Singh R, Suhonen S, Järventaus H, Vanhala E, Catalán J, Farmer PB, Savolainen KM, Norppa H. Genotoxicity of short single-wall and multi-wall carbon nanotubes in human bronchial epithelial and mesothelial cells *in vitro*. Toxicology, 2013, 331(1):24–37.

[64] Snyder-Talkington BN, Dong C, Zhao X, Dymacek J, Porter DW, Wolfarth MG, Castranova V, Qian D, Guo NL. Multi-walled carbon nanotube-induced gene expression *in vitro*: concordance with *in vivo* studies. Toxicology, 2015, 328:66–74.

[65] Fraczek A, Menaszek E, Paluszkiewicz C, Blazewicz M. Comparative *in vivo* biocompatibility study of single- and multi-wall carbon nanotubes. Acta Biomater, 2008, 4(6):1593–1602.

[66] Poulsen SS, Saber AT, Mortensen A, Szarek J, Wu D, Williams A, Andersen O, Jacobsen NR, Yauk CL, Wallin H, Halappanavar S, Vogel U. Changes in cholesterol homeostasis and acute phase response link pulmonary exposure to multi-walled carbon nanotubes to risk of cardiovascular disease. Toxicol Appl Pharmacol, 2015, 283(3):210–222.

[67] Sitharaman B, Shi X, Walboomers XF, Liao H, Cuijpers V, Wilson LJ, Mikos AG, Jansen JA. *In vivo* biocompatibility of ultra-short single-walled carbon nanotube/biodegradable polymer nanocomposites for bone tissue engineering. Bone, 2008, 43(2):362–370.

[68] Wang JTW, Fabbro C, Venturelli E, Ménard-Moyon C, Chaloin O, Da Ros T, Methven L, Nunes A, Sosabowski JK, Mather SJ, Robinson MK, Amadou J, Prato M, Bianco A, Kostarelos K, Al-Jamal KT. The relationship between the diameter of chemically-functionalized multi-walled carbon nanotubes and their organ biodistribution profiles *in vivo*. Biomaterials, 2014, 35(35):9517–9528.

[69] Frank EA, Birch ME, Yadav JS. MyD88 mediates *in vivo* effector functions of alveolar macrophages in acute lung inflammatory responses to carbon nanotube exposure. Toxicol Appl Pharmacol, 2015, 288(3):322–329.

[70] Kafa H, Wang JTW, Rubio N, Venner K, Anderson G, Pach E, Ballesteros B, Preston JE, Abbot NJ, Al-Jamal KT. The interaction of carbon nanotubes with an *in vitro* blood–brain barrier model and mouse brain *in vivo*. Biomaterials, 2015, 53:437–452.

[71] Shvedova AA, Kisin ER, Murray AR, Mouithys-Mickalad A, Stadler K, Mason RP, Kadiiska, M. ESR evidence for *in vivo* formation of free radicals in tissue of mice exposed to single-walled carbon nanotubes. Free Radic Biol Med, 2014, 73:154–165.

[72] Weber GEB, Dal Bosco L, Gonçalves COF, Santos AP, Fantini C, Furtado CA, Parfitt GM, Peixoto C, Romano LA, Vaz BS, Barros DM. Biodistribution and toxicological study of PEGylated single-wall carbon nanotubes in the zebrafish (*Danio rerio*) nervous system. Toxicol Appl Pharmacol, 2014, 280(3):484–492.

[73] Naya M, Kobayashi N, Mizuno K, Matsumoto K, Ema M, Nakanishi J. Evaluation of the genotoxic potential of single-wall carbon nanotubes by using a battery of *in vitro* and *in vivo* genotoxicity assays. Regul Toxicol Pharmacol, 2011, 61(2):192–198.

[74] Naya M, Kobayashi N, Endoh S, Maru J, Honda K, Ema M, Tanaka J, Fukumoro M, Hasegawa K, Nakajima M, Hayashi M, Nakanishi J. *In vivo* genotoxicity study of single-wall carbon nanotubes using comet assay following intratracheal instillation in rats. Regul Toxicol Pharmacol, 2012, 64(1):124–129.

[75] Mihaiescu DE, Grumezescu AM, Buteica AS, Mogosanu DE, Balaure PC, Mihaiescu OM, Trăistaru V, Vasile BS. Bioassay and electrochemical evaluation of controlled release behavior of cephalosporins from magnetic nanoparticles. Dig J Nanomater Biostruct, 2012, 7(1):253–260.

[76] Istrate CM, Holban AM, Grumezescu AM, Mogoantă L, Mogoşanu GD, Savopol T, Moisescu M, Iordache M, Vasile BS, Kovacs E. Iron oxide nanoparticles modulate the interaction of different antibiotics with cellular membranes. Rom J Morphol Embryol, 2014, 55(3):849–856.

[77] Mogoşanu GD, Popescu FC, Busuioc CJ, Lascăr I, Mogoantă L. Comparative study of microvascular density in experimental third-degree skin burns treated with topical preparations containing herbal extracts. Rom J Morphol Embryol, 2013, 54(1):107–113.

[78] Yang Y, Xie L, Chen Z, Liu M, Zhu T, Liu Z. Purification and length separation of single-walled carbon nanotubes using chromatographic method. Synthetic Met, 2005, 155(3):455–460.

[79] Montoro LA, Rosolen JM. A multi-step treatment to effective purification of single-walled carbon nanotubes. Carbon, 2006, 44(15):3293–3301.

[80] Cai Y, Yan ZH, Lv YC, Zi M, Yuan LM. High-speed counter-current chromatography for purification of single-walled carbon nanotubes. Chin Chem Lett, 2008, 19(11):1345–1348.

[81] Zhao B, Hu H, Niyogi S, Itkis ME, Hamon MA, Bhowmik P, Meier MS, Haddon RC. Chromatographic purification and properties of soluble single-walled carbon nanotubes. J Am Chem Soc, 2001, 123(47):11673–11677.

[82] Ansón-Casaos A, González-Domínguez JM, Martínez MT. Separation of single-walled carbon nanotubes from graphite by centrifugation in a surfactant or in polymer solutions. Carbon, 2010, 48(10):2917–2924.

[83] Blanch AJ, Lenehan CE, Quinton JS. Parametric analysis of sonication and centrifugation variables for dispersion of single walled carbon nanotubes in aqueous solutions of sodium dodecylbenzene sulfonate. Carbon, 2011, 49(15):5213–5228.

[84] Shirazi Y, Tofighy MA, Mohammadi T, Pak A. Effects of different carbon precursors on synthesis of multiwall carbon nanotubes: purification and functionalization. Appl Surf Sci, 2011, 257(16):7359–7367.

[85] Pifferi V, Cappelletti G, Di Bari C, Meroni D, Spadavecchia F, Falciola L. Multi-walled carbon nanotubes (MWCNTs) modified electrodes: effect of purification and functionalization on the electroanalytical performances. Electrochim Acta, 2014, 146: 403–410.

[86] Prakash D, Amente C, Dharamvir K, Singh B, Singh R, Shaaban ER, Al-Douri Y, Khenata R, Darroudi M, Verma KD. Synthesis, purification and microstructural characterization of nickel doped carbon nanotubes for spintronic applications. Ceram Int, 2015, Nov 22.

[87] Chen CM, Chen M, Leu FC, Hsu SY, Wang SC, Shi SC, Chen CF. Purification of multi-walled carbon nanotubes by microwave digestion method. Diam Relat Mater, 2004, 13(4–8):1182–1186.

[88] Pełech I, Narkiewicz U, Kaczmarek A, Jędrzejewska A, Pełech R. Removal of metal particles from carbon nanotubes using conventional and microwave methods. Sep Purif Technol, 2014, 136:105–110.

[89] Lin L, Peng H, Ding G. Dispersion stability of multi-walled carbon nanotubes in refrigerant with addition of surfactant. Appl Therm Eng, 2015, 91:163–171.

[90] Mohamed A, Anas AK, Bakar SA, Ardyani T, Zin WMW, Ibrahim S, Sagisaka M, Brown P, Eastoe J. Enhanced dispersion of multiwall carbon nanotubes in natural rubber latex nanocomposites by surfactants bearing phenyl groups. J Colloid Interface Sci, 2015, 455:179–187.
[91] Poorgholami-Bejarpasi N, Sohrabi B. Role of surfactant structure in aqueous dispersions of carbon nanotubes. Fluid Phase Equilibr, 2015, 394:19–28.
[92] Ansari R, Ajori S, Rouhi S. Structural and elastic properties and stability characteristics of oxygenated carbon nanotubes under physical adsorption of polymers. Appl Surf Sci, 2015, 332:640–647.
[93] Liu YT, Wu GP, Lu CX. Grafting of carbon nanotubes onto carbon fiber surfaces by step-wise reduction of *in-situ* generated diazonium salts for enhancing carbon/epoxy interfaces. Mater Lett, 2014, 134:75–79.
[94] Yang G, Zhao F. Molecularly imprinted polymer grown on multiwalled carbon nanotube surface for the sensitive electrochemical determination of amoxicillin. Electrochim Acta, 2015, 174:33–40.
[95] Bencze LC, Bartha-Vári JH, Katona G, Toşa MI, Paizs C, Irimie FD. Nanobioconjugates of *Candida antarctica* lipase B and single-walled carbon nanotubes in biodiesel production. Bioresour Technol, 2016, 200:853–860.
[96] Chen X, Yu X, Liu Y, Zhang J. Stepwise design of noncovalent wrapping of large diameter carbon nanotubes by peptides. J Mol Graph Model, 2013, 46:83–92.
[97] Brković DV, Avramov Ivić ML, Rakić VM, Valentini L, Uskoković PS, Marinković AD. Electrical and morphological characterization of multiwalled carbon nanotubes functionalized *via* the Bingel reaction. J Phys Chem Solids, 2015, 83:121–134.
[98] Fernandes C, Pereira C, Guedes A, Rebelo SLH, Freire C. Gold nanoparticles decorated on Bingel–thiol functionalized multiwall carbon nanotubes as an efficient and robust catalyst. Appl Catal A Gen, 2014, 486:150–158.
[99] Lee KW, Lee CE. Edge-state magnetism in hydrogenated armchair carbon nanotubes. Curr Appl Phys, 2014, 14(12): 1783–1787.
[100] Likozar B, Major Z. Morphology, mechanical, cross-linking, thermal, and tribological properties of nitrile and hydrogenated nitrile rubber/multi-walled carbon nanotubes composites prepared by melt compounding: the effect of acrylonitrile content and hydrogenation. Appl Surf Sci, 2010, 257(2):565–573.
[101] Liu C, Zhang Q, Stellacci F, Marzari N, Zheng L, Zhan Z. Carbene-functionalized single-walled carbon nanotubes and their electrical properties. Small, 2011, 7(9):1257–1263.
[102] Yadav SK, Kim IJ, Kim HJ, Kim J, Hong SM, Koo CM. PDMS/MWCNT nanocomposite actuators using silicone functionalized multiwalled carbon nanotubes *via* nitrene chemistry. J Mater Chem C, 2013, 1(35):5463–5470.
[103] Shanbedi M, Heris SZ, Amiri A, Hosseinipour E, Eshghi H, Kazi SN. Synthesis of aspartic acid-treated multi-walled carbon nanotubes based water coolant and experimental investigation of thermal and hydrodynamic properties in circular tube. Energy Convers Manage, 2015, 105:1366–1376.
[104] Yesil S, Bayram G. Effect of carbon nanotube purification on the electrical and mechanical properties of poly(ethylene terephthalate) composites with carbon nanotubes in low concentration. J Appl Polym Sci, 2011, 119(6):3360–3371.
[105] Gogoi P, Horo H, Khannam M, Dolui S.K. *In situ* synthesis of green bionanocomposites based on aqueous citric acid cured epoxidized soybean oil-carboxylic acid functionalized multiwalled carbon nanotubes. Ind Crop Prod, 2015, 76: 346–354.
[106] Oh JW, Yoon YW, Heo J, Yu J, Kim H, Kim TH. Electrochemical detection of nanomolar dopamine in the presence of neurophysiological concentration of ascorbic acid and uric acid using charge-coated carbon nanotubes *via* facile and green preparation. Talanta, 2016, 147:453–459.
[107] Musumeci AW, Waclawik ER, Frost RL. A comparative study of single-walled carbon nanotube purification techniques using Raman spectroscopy. Spectrochim Acta A Mol Biomol Spectrosc, 2008, 71(1):140–142.
[108] Yaragalla S, Anilkumar G, Kalarikkal N, Thomas S. Structural and optical properties of functionalized multi-walled carbon nanotubes. Mater Sci Semicond Process, 2016, 41:491–496.
[109] Deep A, Sharma AL, Kumar P. Lipase immobilized carbon nanotubes for conversion of *Jatropha* oil to fatty acid methyl esters. Biomass Bioenergy, 2015, 81:83–87.
[110] Hu X, Cheng Z. Removal of diclofenac from aqueous solution with multi-walled carbon nanotubes modified by nitric acid. Chin J Chem Eng, 2015, 23(9):1551–1556.
[111] Yang Q, Pang SK, Yung KC. Dynamic high potential treatment with dilute acids for lifting the capacitive performance of carbon nanotube/conducting polymer electrodes. J Electroanal Chem, 2015, 758:125–134.
[112] Benavides LA, Cuscueta DJ, Troiani H, Ghilarducci AA, Salva HR. Effect of carbon nanotubes purification in the performance of a negative electrode of a Ni/MH battery. Int J Hydrogen Energy, 2014, 39(16):8841–8845.
[113] Choi EY, Choi LW, Kim CK. Noncovalent functionalization of multi-walled carbon nanotubes with hydroxyl group-containing pyrene derivatives for their composites with polycarbonate. Carbon, 2015, 95:91–99.
[114] Boskovic G, Ratkovic S, Kiss E, Geszti O. Carbon nanotubes purification constrains due to large Fe–Ni/Al_2O_3 catalyst particles encapsulation. Bull Mater Sci, 2013, 36(1):1–7.
[115] Ding H, Li X, Wang J, Zhang X, Chen C. Adsorption of chlorophenols from aqueous solutions by pristine and surface functionalized single-walled carbon nanotubes. J Environ Sci, 2015, Nov 28.
[116] Ye Q, Jiang J, Wang C, Liu Y, Pan H, Shi Y. Adsorption of low-concentration carbon dioxide on amine-modified carbon nanotubes at ambient temperature. Energy Fuels, 2012, 26(4):2497–2504.
[117] Su F, Lu C, Chung AJ, Liao CH. CO_2 capture with amine-loaded carbon nanotubes *via* a dual-column temperature/vacuum swing adsorption. Appl Energy, 2014, 113:706–712.
[118] Wu G, Ma L, Liu L, Wang Y, Xie F, Zhong Z, Zhao M, Jiang B, Huang Y. Interface enhancement of carbon fiber reinforced methylphenylsilicone resin composites modified with silanized carbon nanotubes. Mater Design, 2016, 89: 1343–1349.
[119] González-Gaitán C, Ruiz-Rosas R, Morallón E, Cazorla-Amorós D. Functionalization of carbon nanotubes using aminobenzene acids and electrochemical methods. Electroactivity for the oxygen reduction reaction. Int J Hydrogen Energy, 2015, 40(34):11242–11253.
[120] Barabás R, Katona G, Bogya ES, Diudea MV, Szentes A, Zsirka B, Kovács J, Kékedy-Nagy L, Czikó M. Preparation and characterization of carboxyl functionalized multiwall carbon nanotubes–hydroxyapatite composites. Ceram Int, 2015, 41(10 Pt A):12717–12727.
[121] Chiang YC, Lin WH, Chang YC. The influence of treatment duration on multi-walled carbon nanotubes functionalized by H_2SO_4/HNO_3 oxidation. Appl Surf Sci, 2011, 257(6): 2401–2410.
[122] Gorji TB, Ranjbar AA, Mirzababaei SN. Optical properties of carboxyl functionalized carbon nanotube aqueous nanofluids as direct solar thermal energy absorbers. Sol Energy, 2015, 119:332–342.
[123] Mamba G, Mbianda XY, Govender PP. Phosphorylated multiwalled carbon nanotube–cyclodextrin polymer: synthesis, characterisation and potential application in water purification. Carbohydr Polym, 2013, 98(1):470–476.
[124] Cabral DGA, Lima ECS, Moura P, Dutra RF. A label-free electrochemical immunosensor for hepatitis B based on hyaluronic acid–carbon nanotube hybrid film. Talanta, 2016, 148:209–215.
[125] Chen H, Choo TK, Huang J, Wang Y, Liu Y, Platt M, Palaniappan A, Liedberg B, Tok AIY. Label-free electronic detection of interleukin-6 using horizontally aligned carbon nanotubes. Mater Design, 2016, 90:852–857.
[126] Gutierrez FA, Rubianes MD, Rivas GA. Electrochemical sensor for amino acids and glucose based on glassy carbon electrodes modified with multi-walled carbon nanotubes and copper microparticles dispersed in polyethylenimine. J Electroanal Chem, 2015, Oct 28.
[127] Han J, Jiang L, Li F, Wang P, Liu Q, Dong Y, Li Y, Wei Q. Ultrasensitive non-enzymatic immunosensor for carcino-embryonic antigen based on palladium hybrid vanadium

pentoxide/multiwalled carbon nanotubes. Biosens Bioelectron, 2016, 77:1104–1111.
[128] Xiao C, Zou Q, Tang Y. Surface nitrogen-enriched carbon nanotubes for uniform dispersion of platinum nanoparticles and their electrochemical biosensing property. Electrochim Acta, 2014, 143:10–17.
[129] Yeşiller G, Sezgintürk MK. A new methodology for the determination of enzyme activity based on carbon nanotubes and glucose oxidase. J Pharm Biomed Anal, 2015, 115:254–259.
[130] Ding W, Lou C, Qiu J, Zhao Z, Zhou Q, Liang M, Ji Z, Yang S, Xing D. Targeted Fe-filled carbon nanotube as a multifunctional contrast agent for thermoacoustic and magnetic resonance imaging of tumor in living mice. Nanomedicine, 2016, 12(1):235–244.
[131] Ormsby RW, McNally T, Mitchell CA, Musumeci A, Schiller T, Halley P, Gahan L, Martin D, Smith SV, Dunne NJ. Chemical modification of multiwalled carbon nanotube with a bifunctional caged ligand for radioactive labelling. Acta Materialia, 2014, 64:54–61.
[132] Servant A, Jacobs I, Bussy C, Fabbro C, da Ros T, Pach E, Ballesteros B, Prato M, Nicolay K, Kostarelos K. Gadolinium-functionalised multi-walled carbon nanotubes as a T_1 contrast agent for MRI cell labelling and tracking. Carbon, 2016, 97: 126–133.
[133] Wang H, Wang Z, Ye M, Zong S, Li M, Chen P, Ma X, Cui Y. Optically encoded nanoprobes using single walled carbon nanotube as the building scaffold for magnetic field guided cell imaging. Talanta, 2014, 119:144–150.
[134] Cao X, Tao L, Wen S, Hou W, Shi X. Hyaluronic acid-modified multiwalled carbon nanotubes for targeted delivery of doxorubicin into cancer cells. Carbohydr Res, 2015, 405: 70–77.
[135] Mohammadi ZA, Aghamiri SF, Zarrabi A, Talaie MR. A comparative study on non-covalent functionalization of carbon nanotubes by chitosan and its derivatives for delivery of doxorubicin. Chem Phys Lett, 2015, 642:22–28.
[136] Schwengber A, Prado HJ, Zilli DA, Bonelli PR, Cukierman AL. Carbon nanotubes buckypapers for potential transdermal drug delivery. Mater Sci Eng C Mater Biol Appl, 2015, 57: 7–13.
[137] Leilei Z, Hejun L, Kezhi L, Qiang S, Qiangang F, Yulei Z, Shoujie L. Electrodeposition of carbonate-containing hydroxyapatite on carbon nanotubes/carbon fibers hybrid materials for tissue engineering application. Ceram Int, 2015, 41(3 Pt B): 4930–4935.
[138] Mata D, Horovistiz AL, Branco I, Ferro M, Ferreira NM, Belmonte M, Lopes MA, Silva RF, Oliveira FJ. Carbon nanotube-based bioceramic grafts for electrotherapy of bone. Mater Sci Eng C Mater Biol Appl, 2014, 34:360–368.
[139] Ostrovidov S, Shi X, Zhang L, Liang X, Kim SB, Fujie T, Ramalingam M, Chen M, Nakajima K, Al-Hazmi F, Bae H, Memic A, Khademhosseini A. Myotube formation on gelatin nanofibers – multi-walled carbon nanotubes hybrid scaffolds. Biomaterials, 2014, 35(24):6268–6277.
[140] Park S, Park J, Jo I, Cho SP, Sung D, Ryu S, Park M, Min KA, Kim J, Hong S, Hong BH, Kim BS. *In situ* hybridization of carbon nanotubes with bacterial cellulose for three-dimensional hybrid bioscaffolds. Biomaterials, 2015, 58:93–102.
[141] Sun H, Lü S, Jiang XX, Li X, Li H, Lin Q, Mou Y, Zhao Y, Han Y, Zhou J, Wang C. Carbon nanotubes enhance intercalated disc assembly in cardiac myocytes *via* the *β*1-integrin-mediated signaling pathway. Biomaterials, 2015, 55: 84–95.
[142] Ogbodu RO, Limson JL, Prinsloo E, Nyokong T. Photophysical properties and photodynamic therapy effect of zinc phthalocyanine-spermine-single walled carbon nanotube conjugate on MCF-7 breast cancer cell line. Synthetic Met, 2015, 204: 122–132.
[143] Qi X, Rui Y, Fan Y, Chen H, Ma N, Wu Z. Galactosylated chitosan-grafted multiwall carbon nanotubes for pH-dependent sustained release and hepatic tumor-targeted delivery of doxorubicin *in vivo*. Colloids Surf B Biointerfaces, 2015, 133:314–322.
[144] Wu H, Shi H, Zhang H, Wang X, Yang Y, Yu C, Hao C, Du J, Hu H, Yang S. Prostate stem cell antigen antibody-conjugated multiwalled carbon nanotubes for targeted ultrasound imaging and drug delivery. Biomaterials, 2014, 35(20): 5369–5380.
[145] Zhang B, Wang H, Shen S, She X, Shi W, Chen J, Zhang Q, Hu Y, Pang Z, Jiang X. Fibrin-targeting peptide CREKA-conjugated multi-walled carbon nanotubes for self-amplified photothermal therapy of tumor. Biomaterials, 2015, 79:46–55.
[146] Gupta P, Sharan S, Roy P, Lahiri D. Aligned carbon nanotube reinforced polymeric scaffolds with electrical cues for neural tissue regeneration. Carbon, 2015, 95:715–724.
[147] Lee JH, Lee JY, Yang SH, Lee EJ, Kim HW. Carbon nanotube–collagen three-dimensional culture of mesenchymal stem cells promotes expression of neural phenotypes and secretion of neurotrophic factors. Acta Biomater, 2014, 10(10):4425–4436.
[148] Matsumoto K, Shimizu N. Activation of the phospholipase C signaling pathway in nerve growth factor-treated neurons by carbon nanotubes. Biomaterials, 2013, 34(24):5988–5994.
[149] Deng X, Luo M, Shao E, Zhao H, Yang X, Ni Q, Jiao Z. Long-term biodistribution, metabolism and toxicity of carbon nanotubes *in vivo*. Toxicol Lett, 2013, 221(Suppl):S242.
[150] Mohammadi M, Salmasi Z, Hashemi M, Mosaffa F, Abnous K, Ramezani M. Single-walled carbon nanotubes functionalized with aptamer and piperazine–polyethyleneimine derivative for targeted siRNA delivery into breast cancer cells. Int J Pharm, 2015, 485(1–2):50–60.
[151] Siu KS, Chen D, Zheng X, Zhang X, Johnston N, Liu Y, Yuan K, Koropatnick J, Gillies ER, Min WP. Non-covalently functionalized single-walled carbon nanotube for topical siRNA delivery into melanoma. Biomaterials, 2014, 35(10): 3435–3442.

Corresponding author
Dan Eduard Mihaiescu, Chem. Eng., PhD, Department of Organic Chemistry, Faculty of Applied Chemistry and Materials Science, Politehnica University of Bucharest, 1–7 Polizu Street, 011061 Bucharest, Romania; Phone +4021–402 39 97, e-mail: danedmih@gmail.com

Received: April 21, 2015

Accepted: December 18, 2015